Molecular Chirality Detection via Optical Rectification in Spin-Momentum Locking

By

Jessie Rae Rapoza

Sc.B., Brown University, 2021

Thesis

Submitted in partial fulfillment of the requirements for the
Degree of Master of Science in Biomedical Engineering at Brown University

PROVIDENCE, RHODE ISLAND

MAY 2022

This thesis by Jessie Rae Rapoza is accepted in its present form

by the Center of Biomedical Engineering as satisfying the

thesis requirement for the Degree of Master of Science.

Date_____ _____

Dr. Jimmy Xu, Advisor

Recommended to the Graduate Council

Date_____ _____

Dr. Marissa Grey, Committee Member

Date_____ _____

Dr. Celinda Kofron, Committee Member

Approved by the Graduate Council

Date_____ _____

Andrew G. Cambell, Ph.D.
Dean of the Graduate School

Acknowledgements

I would like to thank my advisor, Dr. Jimmy Xu, for being such an incredible guide on this journey for me. You forced me to begin the process of regaining the confidence in myself that I had lost during my undergraduate years. You also imparted a sense of respect, professionalism, and work ethic that I will take with me forever.

I also owe a gigantic thank you to another mentor, Dr. Petr Moroshkin. Without your aid I would never have completed this thesis. I greatly appreciate all of the time you dedicated to teaching me and guiding my research development.

To my parents who have been with me through my highest and lowest points: you are my best friends and by biggest supporters. I could not have made it this far without your love and guidance.

A final thank you to my friends and the entirety of the Xu Lab, I feel blessed to be supported by so many incredible people, and to the support to our lab's Optical Rectification exploration from AFOSR FA9550-19-1-0355.

Table of Contents

List of Tables and Figures

Chapter 1: Introduction

1.1 Chirality

Chirality is a phenomenon which describes a non-superimposable configuration of objects with mirrored, identical compositions. The age-old example of a pair of hands is an effective method of conceptualizing chirality. A hand is almost an exact replica of its partner, except in that left and right cannot be superimposed on each other. The very word, "chiral," is rooted in this idea, as it comes from the Greek root "kheir," translating in English to "hand"[1].

Chirality exists all around us, on every scale of magnitude, and in every field of science. At the subatomic level, electrons are one example of this phenomenon due to their existence in a state of either spin up or spin down. Though these small particles share the same composition, they differ in their interactions with surrounding environments[2,3]. On the other end of the spectrum, chirality also exists in the cosmos. The chiral phenomenon of circularly polarized light (CPL) is known to be emitted from many astronomical sources, including reflection nebulae[3], light reflected off of planets[5], and gamma-ray bursts[6]. CPL is configured in a distinct corkscrew-like shape with either clockwise or counter-clockwise orientations; these non-superimposable mirrored arrangements result in the classification of CPL as chiral entities. Today, many believe that the existence of this CPL in our cosmos may be responsible for the enantiomeric excess and homochirality that is characteristic of many of the chiral biomolecules found on and in Earth and its constituents[4,7].

At the intersection of these various perspectives of chirality, a new multidisciplinary understanding of chiral interactions is just developing with the potential for broad and profound impact. Developments such as utilizing electron spin as a tool to induce enantioselective molecular reactions[8], and using CPL to control the spatial orientation of chiral molecules[9] have been described. Advancements of this sort take advantage of the intriguing interactions of chiral entities, which set them apart from one another and from all else. In fact, chiral objects (at least those which are unobservable by the naked eye) are only distinguishable in their exchanges with their surroundings. The more that scientists become able to understand and exploit these intricacies of the natural world, the further we will be able to push the evolution of technology and medicine. The research described in this thesis addresses another juncture of chiral forms, particularly observing a revealing interaction between surface plasmon polariton (SPP) waves and chiral molecules.

1.2 Distinguishing Chirality

As previously mentioned, one class of chiral objects is enantiomers which are mirror-image pairs of molecules that have identical compositions, making them indistinguishable from one another by their scalar properties. This means that typical defining values such as molecular weight, density, melting point, and so on cannot be used to distinguish between their chiral handedness which however can be greatly consequential in life and in medicine, as described below. In order to make the distinction, vector quantities are necessary due to the inherent directionality of chiral phenomena. For this reason, the interactions experienced between chiral entities and their surroundings allow for chiral handedness to be distinguished due to the vector nature of the forces underlying the interactions.

1.3 Mirror Symmetry Breaking

Nearly synonymous with the notion of chirality is that of symmetry breaking. Symmetry breaking describes an occurrence in which a configurational bias becomes imposed on an object or system, causing it to no longer be symmetric. By definition, any chiral object or system has a broken mirror symmetry.

1.4 Enantiomeric Excess

Many of the building blocks of life, such as amino acids and carbohydrates exist in two mirrored chiral configurations, or enantiomers. However, such biomolecules are almost never naturally found with equivalent concentrations of both left and right chirality[10], known as a racemic mixture. Instead, the typical arrangement of enantiomeric molecules has the concentration of one enantiomer greatly out-weighing the other, or even entirely dominating the scale. In the case of naturally occurring amino acids, the vast majority appear in the left-handed form of the enantiomer, known as the levorotary configuration (stemming from the Latin word for "left", laevus), and annotated with a capital L ("L-amino acid"). Meanwhile the majority of carbohydrates appear in the right-handed form of the enantiomer, or dextrorotary configuration (stemming from the Latin word for "right", dexter), annotated with a capital D ("D-carbohydrate" or "D-amino acid"). This non-racemic distribution of enantiomers is referred to as "enantiomeric excess," and is postulated to be a requirement for life[11].

Homochirality is imbedded in the very architecture of life, granting it an essential role in the functionality and facilitation of any molecular composition. In its absence, the helical (and likewise homochiral) structure of RNA and DNA could never be constructed, let alone undergo

transcription or store genetic information[12]. However, this is not to say that D-amino acids, L-carbohydrates, and other non-preferential chiral molecules do not have a presence in life, or even that they are entirely nonfunctional (which was the accepted school of thought until the mid-late 20th century[13]). Additionally, a synthetic chemistry perspective of molecular syntheses generally observes no chiral preference, producing racemic solutions. This observation only adds to the mystery of the origin of homochirality. Furthermore, racemic mixture production can also be problematic for studying the intricacies of biomolecular interactions which have a natural chirality bias, and for the development of drugs. As such, the ability to detect chiral handedness is necessary for understanding biomolecular processes.

Chapter 2: Background

2.1 Biomolecular Chiral Interactions

Molecular structures dictate how molecules interact with each other, which is a concept that holds true when it comes to stereochemistry. In fact, a difference presents itself in the Gibbs free energy between enantiomers and available interaction molecules[14]. Therefore, chiral handedness plays an important role in the attractive and repulsive forces of molecular interactions. One well accepted model for describing chiral interactions is referred to as the "three-point (minimum) interaction model"[15, 16]. This model states that all chiral exchanges can be described by at least three spatially-dependent points of interaction between one enantiomer and its receptor. These interactive forces can be either attractive or repulsive; it is necessary that all three interaction points occur at once, which is only feasible for one enantiomeric configuration (Figure 1). It has also been noted that instances of large, rigid aromatic π-complex associations can appear to create a two-point interface with similarly rigid chiral molecules, which fully describes enantiomeric dependence. However, defining a molecular interaction in this way is still consistent with the three-point model as soon as a third point in the system is defined to satisfy the necessary components to describe a plane[17].

Figure 1.

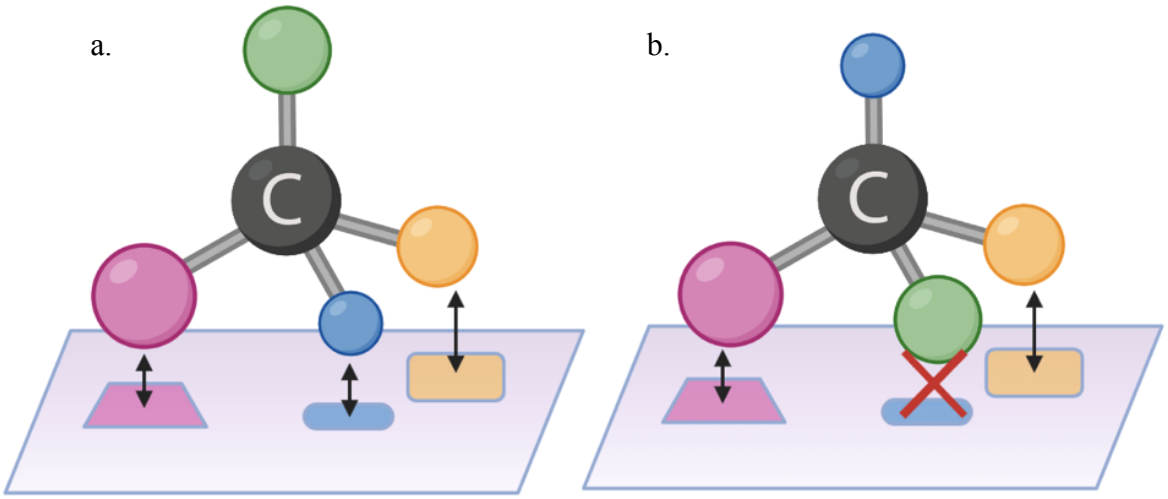

Figure 1. Chiral molecule a interacts with a chiral receptor according to the three-point model. The enantiomer of molecule a, molecule b, is unable to fulfill the three-point interaction model and is unable to create a sufficient bond with the receptor.

As such, every interaction between two chiral components will inherently select for one enantiomer over another. Bearing in mind the magnitude of the presence of chiral molecules and constituents within the body, this widespread enantioselectivity is not a trivial concept. In addition to the amino acids, sugars, and nucleic acids that have already been discussed, protein structures including hormones, enzymes, and transport proteins can all be chiral. Even cells as a whole have been described to have a distinct chirality[18], though, there has not yet been any discussion on how this may impact chiral molecular interactions and transport. The enantioselectivity that is inherent to the inevitable interactions amongst each of these chiral structures prompts significant functional effects. For instance, one chiral molecule may experience attractive forces with a particular transport protein and undergo active transport past a cellular membrane, meanwhile, the enantiomer of said molecule may experience the opposite effect and subsequently be subject to the much more leisurely processes associated with passive transport.

2.2 Implications in Health and Medicine

a) Pharmacology/Toxicology

The previously described notion that molecular functionality is enantiomerically dependent is of great significance when considering pharmaceuticals. While one enantiomer of a drug is intended to perform some sort of beneficial activity, the functionality of the opposite enantiomer usually ranges from being completely inactive, to causing toxic effects in the recipient. An extremely small percentage of drugs share equal roles in bioactivity between enantiomers[19].

Likely the most commonly described example of enantiomerically-based pharmaceutical error is the case of Thalidomide, a drug prescribed to pregnant women to as a treatment for morning sickness in the mid 20th century. Unfortunately, the negative effects of this drug resulted in severe physical birth defects of their babies, including missing and/or not fully formed limbs. Thalidomide, was manufactured and distributed as a racemic mixture, and the two extremely different effects of the drug were caused by the different activities of the two enantiomers (figure 2). The experience from this case, among others, along with an ever-growing understanding of the scientific world, has taught scientists the importance of maintaining an awareness of chirality. Additionally, the US Food and Drug Administration requires that the enantiomeric composition of pharmaceuticals be described as a prerequisite for drug approval[20]. As such, the development of new technologies which may improve the current state of enantiodetection capabilities is a frontier of great interest.

Figure 2.

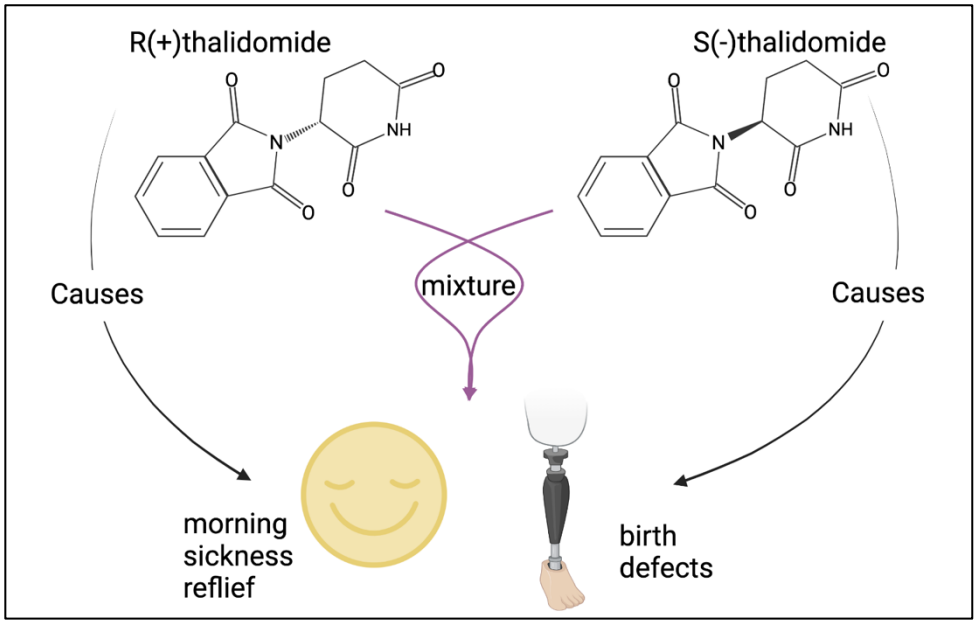

Figure 2. Right-handed thalidomide, "R(+)thalidomide," was an effective treatment for morning sickness experienced by pregnant women. Left-handed thalidomide, "S(-)thalidomide," was responsible for causing birth defects resulting in missing or disformed limbs. A racemic mixture of the two enantiomers was prescribed to patients, resulting in the expression of both effects.

On top of the intrinsic functionality variances between enantiomers, it is also possible for the chirality of a molecule to be flipped after the drug has been administered to a patient[21]. This effect, known as "chiral inversion," could cause unknown consequences if the mechanisms for each drug are not well understood, however, chiral inversion can prove particularly challenging to observe in vivo. This challenge adds additional incentive for the need to develop creative new chirality-sensing measures.

b) Biotechnology Development

In addition to the established necessity to maintain an awareness of pharmaceutical enantiomeric activities, molecular chirality is proving to play another significant role in the realm of drug delivery. Scientists and engineers have discovered that it is possible to take advantage of the enantiomeric dependence of biomolecular interactions. Replacing L-amino acids with D-amino

acids in drug backbones and nanoparticles greatly increases the half-life of such drugs in human plasma[22,23]. These developments can be exploited to fine-tune target site homing, metabolic rates, and overall drug functionality. The developmental processes associated with fashioning this biotechnology necessarily require a method of enantiomeric verification—a practice which is currently not as simplistic as one would hope (see "Current Standards").

c) Diagnostics

Although D-amino acids were long thought to be inactive in the human body, researchers have recently decided to look into the implications that these right-handed molecules may prompt on one's health. Studies show that evaluating enantiomeric ratios of amino acids provides the potential to evaluate ageing and disease states[24]. More specialized findings from similar studies have suggested a correlation between both amyotrophic lateral sclerosis (ALS) and schizophrenia with abnormally high and abnormally low respective concentrations of D-serine[25,26]. One diagnostic hope driven by these findings is the potential for a threshold-based enantiomeric detection method to aid in the identification of ALS and schizophrenia. As ALS diagnostic procedures, such as an electromyogram, can be extensive and uncomfortable ordeals, and the repertoire of schizophrenia diagnostic tools currently does not include a single physiological measure, a detection method utilizing D-amino acids could greatly improve the diagnostic timeline and accuracy for both conditions.

In addition to the potential neurological diagnostic implications, it may also be conceivable that enantiomeric ratios of amino acids could aid in the detection of cancer cells. An in vitro study which analyzed such relations in both healthy and cancerous breast epithelial cells reportedly observed a significant increase in D-aspartic acid and D-serine concentrations in the breast cancer cells as compared to the healthy cells[27]. A separate ex vivo study evaluated the relation between

cases of hepatocellular carcinoma and amino acids in human serum. The findings of this study depict a potential correlation between abnormally low concentrations of D-glutamine and D-glutamic acid in human serum, with the incidence of hepatocellular carcinoma[28]. In conjuncture with these findings, the development of novel enantiomeric detection methods could potentially lead to earlier diagnoses, greatly improving patient outcomes and quality of life.

d) Supramolecular Structure Analysis

The act of characterizing chirality is of great importance not only for individual molecules, but also for supramolecular structures. In particular, an analysis protein structures, which are comprised of chiral amino acids, uncovers vital information regarding functionality. From the enzymes that catalyze reactions, to the hormones that regulate body systems, to the transport proteins that act as cellular gate keepers, each of these functions are driven by interactions which are dependent on the chirality of these proteins. As such, chiral structural analyses of proteins provide an avenue for scientists to develop a deeper understanding of the driving forces which dictate these essential biomolecular processes, furthermore, creating a platform to recognize how and why such processes may or may not occur.

2.3 Current Standards of Chirality Detection

Currently there are many standard methods for analyzing chiral handedness, however, each of these methods require bulky, costly equipment, greatly reducing the accessibility of this form of analysis.

i. Liquid Chromatography/Mass Spectrometry (LC/MS)

LC/MS is a molecular analysis method that provides readouts of atomic compositions of a desired solution. This method functions by first passing a liquid solution through a

group of small, high surface area columns, intended to separate out mixture components. This stage of the process is known as liquid chromatography and is the more important component when considering chirality detection. The second stage is known as mass spectrometry and is responsible for the atomic composition identification from the separated mixture components. This process usually utilizes electrospray ionization to measure mass-to-charge ratios of individual ions, identifying each atomic constituent along with its relative abundance.

The most common method of liquid chromatography separates constituents by polarity. In this method, the columns are loaded with either polar or non-polar beads that the solution is forced to interact with upon passage through the columns, however, there are many forms of liquid chromatography. The two described methods (of polar stationary phase and non-polar stationary phase) are known as normal phase and reverse phase liquid chromatography, respectively. Meanwhile, other common forms include ion exchange and size exclusion. Over all, every liquid chromatography method functions by separating molecular constituents into a mobile phase, which readily passes through the columns, and a stationary phase, which experiences attractive forces within the columns, causing this phase to remain in the columns for a longer duration than the mobile phase.

There is more than one way that liquid chromatography can be implemented as a chiral selection tool. The first possibility is to utilize the traditional, achiral forms of liquid chromatography, but to first add a "chiral mobile phase additive"[29]. This additive would ideally exploit the chiral handedness of the target solution, while simultaneously creating a bias towards the mobile phase. As a result, one enantiomer will bind to the additive and

quickly be processed through the liquid chromatography columns, meanwhile, the other enantiomer will be associated with the stationary phase.

In contrast, the other option to separate enantiomers is to use a chiral stationary phase (CSP). In general, CSP methods utilize the previously described three-point interaction model for chiral molecules. Chirality dependent interaction sites are localized in the columns for the racemic solution to cross paths with. Though the basis for this concept appears rather simplistic, the method requires a decent proficiency in biochemistry to navigate in an effective manner. Types of CSPs include: polysaccharide-based, protein-based, cyclodextrin-based, macrocyclic-based, Pirkle-type, Ion-exchange-type, crown ether-based, and cyclofructan-based[30]. Each of these CSP formats is associated with their own mechanisms of interactions, subsequent indications for use, and expected results.

ii. Gas Chromatography/Mass Spectrometry (GC/MS)

GC/MS functions in almost the same way as LC/MS, however, the mobile phase is gaseous instead of liquid. Additionally, there is some variation in the two methods in terms of the forms of CSP. Types of CSPs for GC/MS include: cyclodextrin-based, chiral amino acid-based, metal coordination complexes, chiral ionic liquids, polysaccharide-based, cyclopeptide-based, metal organic frameworks, porous organic cages, and cyclofrucatan-based[31]. LC/MS has the potential to analyze a broader range of compounds in comparison to GC/MS, and the sample preparation when using LC/MS is generally more minimal that that of GC/MS[32]. However, GC/MS costs tend to be significantly less expensive than those associated with LC/MS.

iii. Circular Dichroism Spectroscopy

One of the intriguing properties of chiral molecules can be observed when CPL is directed at an enantiomeric excess solution of the molecules in question. When this action is performed, a wavelength-dependent variance in the magnitude of light absorbed by a chiral molecule, in comparison with its enantiomer, presents itself. This effect is known as circular dichroism. Circular dichroism spectroscopy utilizes this property to characterize chirality. This form of spectroscopy directs a spectrum of wavelengths for both left and right CPL through a transparent enantiomeric solution, and detects the intensity of light that has passed through. From this data, the absorbance can be measured at each wavelength and a graphical representation of this information is used either in comparison with known circular dichroism spectra, or between enantiomers to get a sense of chirality characterization.

iv. Roman Optical Activity

Like circular dichroism, optical rotation is an effect which occurs as a result of incident polarized light. In this case, a solution of chiral molecules will rotate the plane of polarization of linearly polarized light directed at the solution, an effect which can be detected by polarimeter devices. Every chiral molecule has a known value of "specific rotation," which is described by the following equation:

$$[\alpha]_{\lambda}^{T} = \frac{\alpha_{observed}}{c \times l}$$

where, $[\alpha]$ is the specific rotation (dependent on temperature (T) and wavelength (λ)), $\alpha_{observed}$ is the experimentally observed rotation, c is the concentration of the molecule in question (usually in units of g/ml), and l is length of the light that passes through the

solution (usually in units of dm). Enantiomers have specific rotation values with opposite signs, cancelling out the optical rotation effect in the case of a completely racemic solution.

Overall, the current standards for chirality detection and characterization involve multi-step processes and require significant supplementary knowledge for proper usage and evaluation. These methods leave room for user error. Additionally, these pieces of equipment can be very large and bulky, and costs can be overwhelmingly large (Table 1)—two very important pitfalls of these devices which greatly reduce accessibility.

Table 1.

Method	Cost Analysis
LC/MS	• Approximate cost of machinery - $75,000-$1,500,000. • Cost of yearly servicing - approximately $30,000/year/instrument.[33] • Cost of two technologists – approximately $225,000/year.[33]
GC/MS	• Approximate cost of machinery - $50,000-$150,000. • Similar servicing and technologist costs as LC/MS.
Circular Dichroism Spectroscopy	• Approximate cost of machinery - $50,000-$100,000.
Optical Activity	• Approximate cost of machinery - $14,000-$38,000.[34]

Chapter 3: Experimental Background

3.1 Aim

The aim of this research is to propose and present evidence for the feasibility of an electrically-based method of chiral handedness detection. The inspiration for this goal comes from the Xu Lab's recently developed optical rectification mechanism which facilitated the electrical detection of optical spin-momentum locking—a phenomenon associated with the excitation of surface plasmon polariton (SPP) waves by circularly polarized light and their localization to unidirectional propagation along the surface. This system functions by directing a circularly polarized light at an asymmetric, periodically-patterned, metallic surface grating. The resulting effect of this interaction is a net DC drift current, accumulated from the electron plasmonic-oscillations of the generated SPP wave, as a consequence of mirror symmetry breaking from the CPL and asymmetric metallic surface (Figure 3). The direction of the SPP wave and DC current is dependent on the handedness of the incident CPL. The DC current is then detectable by electrodes placed in a line of contact with the grating.

Figure 3.

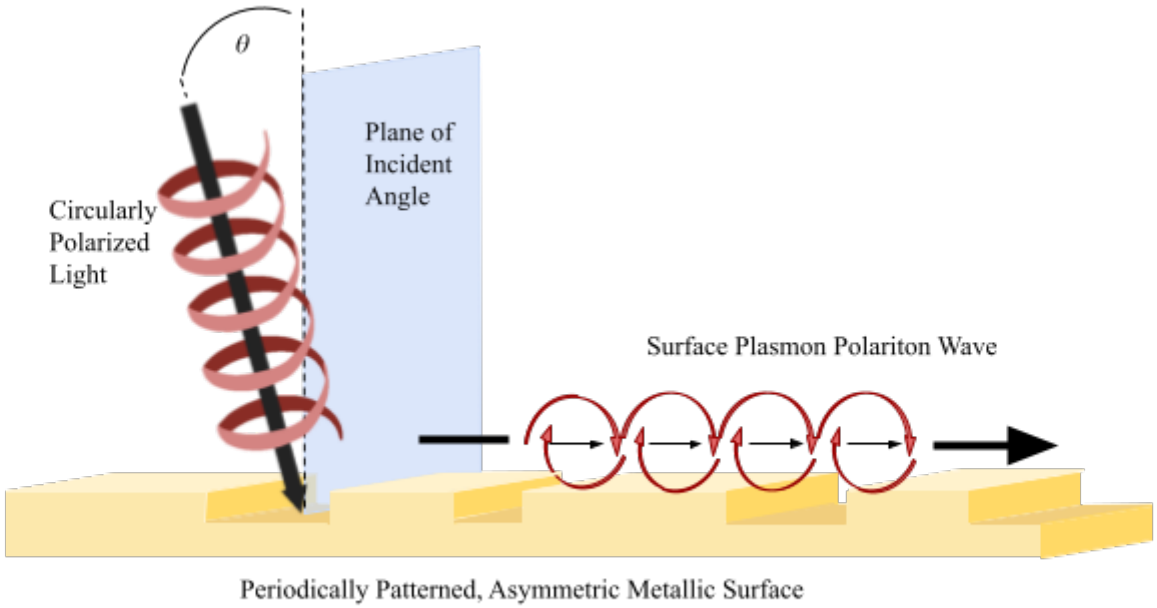

Figure 3: Circularly polarized incident light and the asymmetric, periodically patterned metallic surface create a SPP wave and net DC current by way of mirror symmetry breaking.

In effect, the described system, essentially, simultaneously creates and detects a chiral modality (the SPP wave itself has a spin momentum along the surface and perpendicular to the propagation direction, as such it is chiral). It, therefore, sets the stage for a perfect chiral handedness detection tool, as it meets the two prerequisites that have mandated every chirality recognition mechanism that has been described thus far: 1) a platform for the chiral molecule in question to interact with another chiral entity, and 2) a method to analyze the effects of said interaction. Perhaps the intriguing phenomenon of this system is the duality in which the interaction mechanism and the detector are actually one and the same. As a result, the decision was made to introduce chiral molecules to the metallic surface and perform measurements to determine if a detectable, enantioselective interaction occurs between the SPP wave and the molecules (Figure 4).

Figure 4.

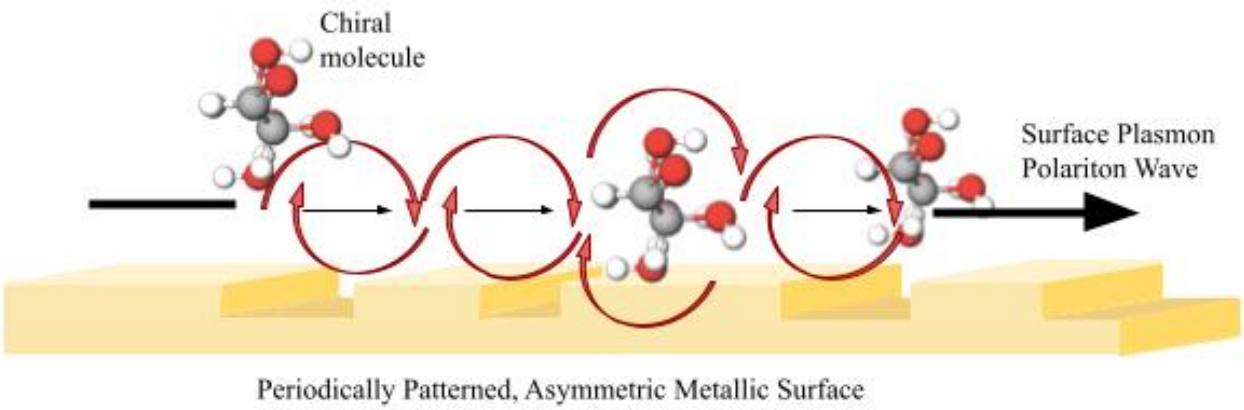

Figure 4. Chiral molecules added to the surface of the metallic grating interact with the SPP wave. Although not depicted here, CPL is still present in this system and necessary for the SPP wave induction.

3.2 Chirality of the SPP Wave

Although SPP waves having chirality is not a commonly addressed notion, the success of this study is dependent upon this claim being true. The first indicator of SPP chirality is the inherent spin momentum vector of SPP waves. As previously noted, spin is a chiral phenomenon. Additionally, chirality has been described in this paper as being the result of mirror symmetry breaking, which is also responsible for the SPP wave in this system, due to the chirality of the incident CPL, the non-normal angle of incidence of the CPL, and the asymmetry of the surface grating.

3.3 Chiral Molecule – SPP Interactive Energy Coupling

Due to the lack of defined interaction sites between the chiral molecules and the SPP wave, as can be described by the three-point interaction model between two solid chiral objects, it is important that a theory be proposed for the interaction mechanism at play. This proposal is that

the charge density wave of the SPP results in a force that is a vector and rotating (spinning), and therefore a coupling and energy exchange between the SPP wave and chiral molecule of 'like' chirality. This model does not assume that there is zero coupling between the SPP and molecule of opposite chiral handedness, however, the coupling expressed in the alike chirality case should be significantly greater. Although the coupling occurs on a molecularly scaled interaction level, it is electrically detected by the optical rectification current, with a magnitude dependence on the intensity of the coupling.

This coupling effect is made possible due to the SPP wave's natural electron plasmonic-oscillations, in conjunction to the net DC drift of the system. As an intrinsic feature of the SPP wave, the oscillating electrons naturally form periods of greater and lesser election densities, in a manner characteristic of a longitudinal wave (Figure 5). The spatial variation of these electron densities creates dipoles (and multipoles) which produce a chiral field in a so-called non-radiative near-field zone and coupling with the chiral molecule. As such, an enantiomer with handedness alike to that of the propagating chiral SPP wave will naturally be favored than the opposite enantiomer. The resulting energy transfer of the preferred enantiomer with the SPP wave will be greater than that resulting from the less favorable enantiomer.

Figure 5.

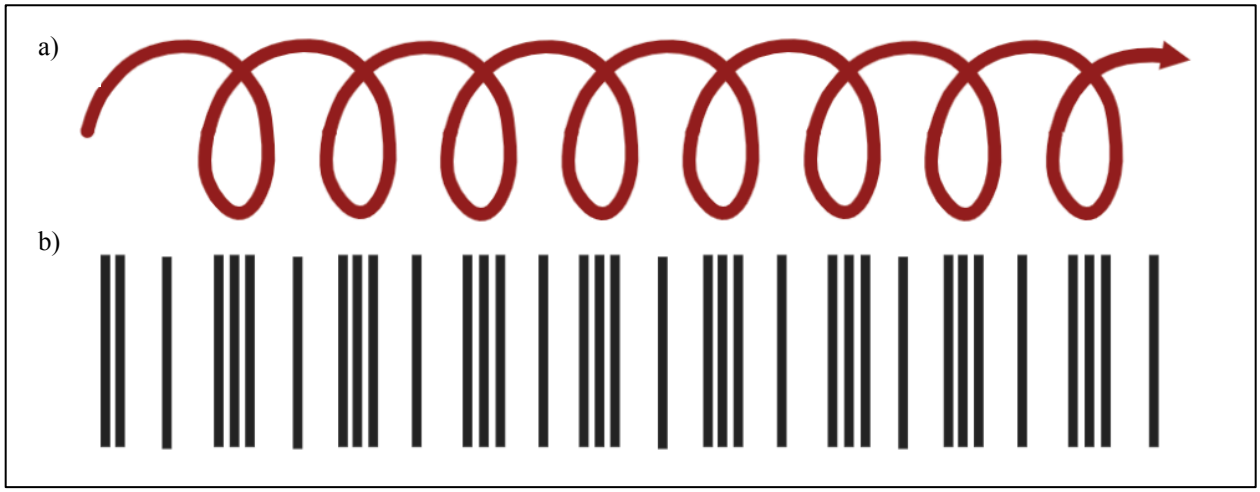

Figure 5. a) Spacing of SPP wave oscillations due to net DC drift current. b) Representation of electron-dense regions of the SPP wave.

The coupling mechanism described, therefore, has the ability to create a distinction between two enantiomeric molecules. For instance, if the right-handed SPP wave is present, then the introduction of the right-handed molecular enantiomer will induce a greater coupling and exchange of energy and therefore a greater modulation of the subsequent DC current, than would be observed with the introduction of the left-handed molecular enantiomer. The opposite is also true if the left-handed SPP wave is present.

3.4 Near-field Zone

Another important note is the mechanism which allows for the induced SPP wave to be detectable at. This mechanism is the evanescent nature of the SPP wave and its field greatly intensified over that of the incident light (up to 10^4) in the near-field zone on the metallic surface. This near-field zone is only approximately 10nm thick, effectively concentrating the energy of the

SPP wave into this confined space, amplifying the interaction with a trace amount of molecule (or, sensitivity).

Chapter 4: Experimental Design

4.1 Arabinose

The chiral molecule utilized to perform all experimentation is the plant-derived carbohydrate, arabinose (Figure 6). One of the attractive features of arabinose is that it is one of the only carbohydrates which exists with a natural enantiomeric excess of its left-handed form. For this reason, it can be less expensive to purchase both enantiopure forms of this molecule in comparison to pretty much all other carbohydrates which tend to be sold for high prices in their L-carbohydrate forms. Additionally, this saccharide is relatively well studied by the scientific community due to an interest in the L-arabinose operon, araBAD[35]. Therefore, important data and properties of the molecule are relatively easy to access.

Figure 6.

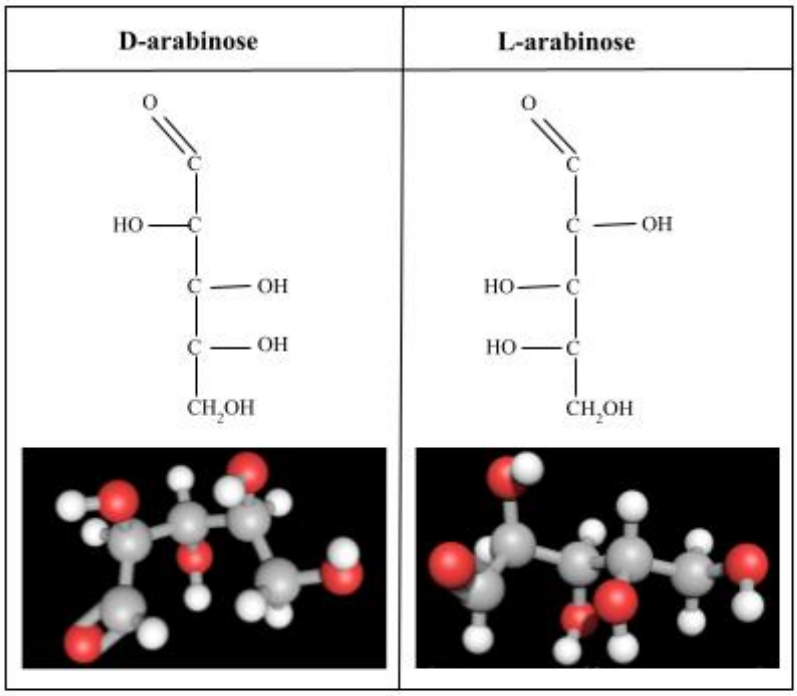

Figure 6. Representation of the structure for D- and L- arabinose with both skeletal structure drawings and 3-dimensional illustrations of possible arrangements.

4.2 Setup

The first component of the experimental setup is a 1064nm cw laser, which is focused through two lenses, then directed through a chopper rotating at a frequency of 128 Hz, a half-wave ($\lambda/2$) plate to ensure uniform polarization, then a quarter-wave ($\lambda/4$) plate to induce an adjustable circular polarization, and finally the light is focused through a lens once more before shinning on the sample (Figure 7). The sample is also comprised of multiple components. The small metallic surface is secured with the gratings oriented horizontally inside a 17.5mL glass cuvette (Figure 8). Along with the metallic surface, a solution of approximately 1.82M enantiopure arabinose in water is introduced into the cuvette and finally two electrodes are clipped to the metallic surface to obtain

electrical current readings. A microscope is also simultaneously directed at the sample, as a tool to gauge the placement of the laser spot on the grating.

Figure 7.

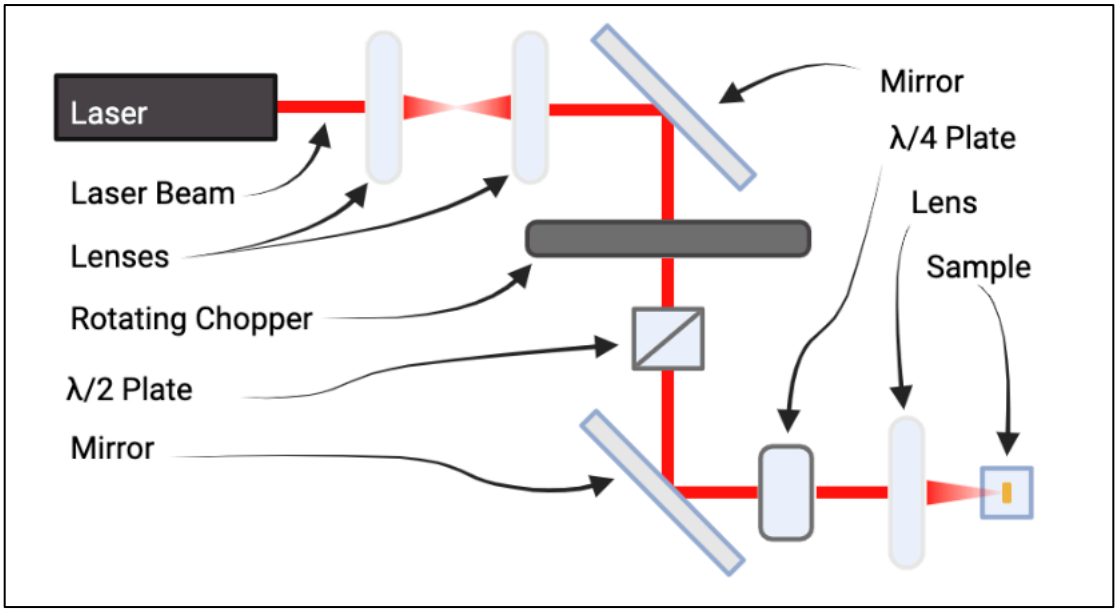

Figure 7. Experimental setup for laser beam path.

a) Metallic Surface Grating

The metallic surface grating is composed of a periodic sequence of groves etched into a multi-layered gold film. The pattern for each unit cell of this grating was previously optimized to produce the greatest optical rectification current. The dimensions for one individual unit cell are represented in Figure 8.

Each gold surface sample was fabricated by first lithographically depositing a gold film on a glass plate. A layer of PMMA (polymethyl methacrylate) was then deposited over the top in a 200nm thick layer and electron-beam lithography was used to pattern the grating. A second gold film layer was placed and then the appropriate pattern was lifted off, creating a two-tiered gold

pattern. The complete size of the grating spans 200µm wide in the direction parallel to the grooves, and almost 450µm long in the direction perpendicular to the grooves.

Figure 8.

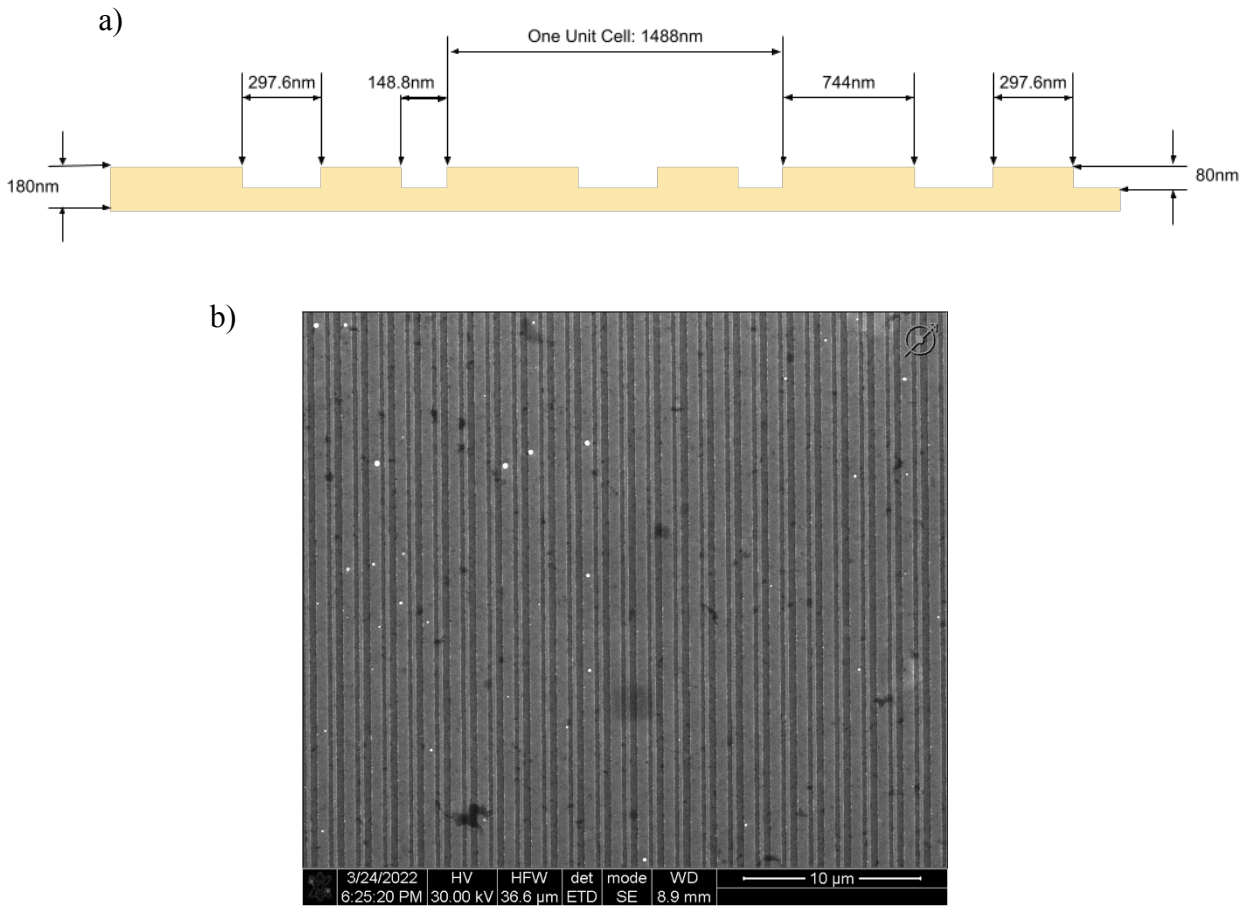

Figure 8. a) Cross-sectional view of three grating unit cells with dimensions. b) Scanning electron microscope image of the gold sample.

b) Arabinose Solution

Enantiopure arabinose solutions were formulated by adding 3.00g (± 0.01g) of either L- or D-arabinose to a small beaker, along with 11.00mL (± 0.02mL) of deionized water, and stirred

until fully dissolved. This concentration is about 2.5x smaller than the supposed solubility threshold of arabinose at room temperature,[33] however, the approximate 1.82M solution was sufficient for obtaining results and ensured that the solution would not contain over-saturation particles which would negatively impact measurements.

c) Axial Sample Rotation

Prior experimental data of the lab has shown that the maximum enantiodetective potential for this system is realized when the incident CPL is angled with respect to the direction of the grooves. This aligns the spin momentum of the incident CPL to that of the SPP (Figure 9a), and thereby selectively excites that SPP propagating in one direction (Figure 9b). For this reason, the cuvette sample is placed on an adjustable stage which allows for the rotation of the sample along the axis perpendicular to the grooves, so that the laser beam may remain stationary while introducing an angled incidence of the light on the sample (Figure 9c). Before experimentation, the angle of incidence at which the greatest desired value of the optical rectification current is produced is unknown. Therefore, data is collected at a range of incident angles in order to encompass the maximal result.

Figure 9.

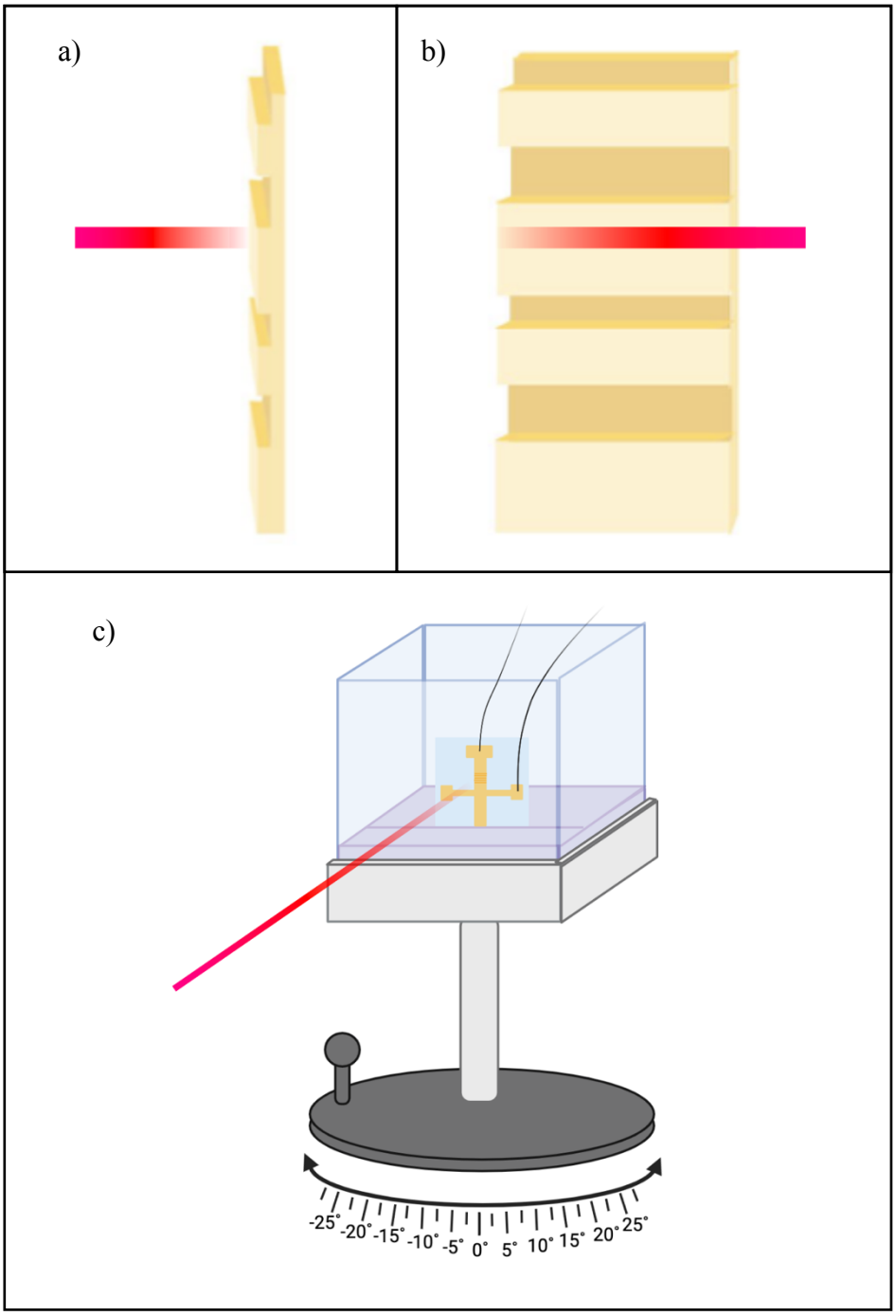

Figure 9. a) Laser beam at normal incidence to the gold surface grating. b) Laser beam aligned in parallel with the surface grating. c) Sample setup in cuvette with vertical rotational axis.

4.3 Procedure

a) Alignment and Beam Width Measurement

The first step of the experiment was to ensure the proper alignment of the laser and adjust any component as necessary. To measure the width of the laser beam, the sample was removed from the laser's path and replaced by a vertically oriented razor blade, blocking the path of light to a photodetector situated on the other side of the razor. The razor was then moved in incremental small steps along the horizontal direction, slowly allowing the laser's path to reach the photodetector. At each step a value for the intensity of the laser's light was recorded from the photodetector. This data was then fitted with a gaussian model to characterize the size and shape of the laser beam, which is beneficial for understanding how the laser interacts with the sample.

b) Demonstrating Experimental Reproducibility with Cuvette

This portion of the experiment was performed to evaluate the experimental setup and ensure that it is possible to replicate the findings of the previous study which serves as the basis for this one, even with the introduction of a cuvette that was not a previous experimental component. No arabinose molecules were used in this experiment. The gold grating was placed in the cuvette, with only air surrounding it. The initial orientation of the cuvette and gold sample was aligned with the laser at a normal angle of incidence to the grating. Minor vertical and horizontal locational adjustments of the laser and sample were made until the laser landed on the spot on the grating which produced the largest observable DC current. Measurements of the optical rectification current for both left and right CPL were recorded at this angle before rotating the cuvette and sample clockwise by 5˚ around the vertical axis and recording again. This process was continued, measuring at 5˚ intervals until the final measurement at 60˚ past normal incidence. Once

completed, this experiment was then repeated with water filling the space around the gold sample, inside the cuvette.

c) Enantiomeric Detection

Arabinose solutions were finally introduced for this experiment. The approximate 1.82M solutions of both L- and D-arabinose were formulated as described above. The gold sample was placed into an empty cuvette, and the space was then carefully filled by one of the two solutions. Just as in the previous experiment, the laser was directed at the sample at normal incidence and its location spot on the grating was carefully adjusted until the sweet-spot was found, producing the largest possible value of optical rectification current. A measurement of both left and right CPL was recorded at normal incidence, before recording subsequent measurements at every 5˚ of clockwise rotation until reaching 60˚ from normal incidence. Upon completion, the cuvette and its constituents were thoroughly rinsed with deionized water and dried using a flow of Nitrogen gas, before reassembling the cuvette setup with the opposite enantiomeric solution this time. The laser and cuvette were realigned very carefully, making and effort to locate the exact same spot as before. Finally, all of the measurements were performed again with the new solution.

Chapter 5: Analytical Methods

Four different experimental conditions were necessary for data collection (right CPL, right molecule / left CPL, right molecule / right CPL, left molecule / left CPL, left molecule). As described previously, the greatest magnitude of optical rectification current should be produced from conditions of like chirality. Therefore, at normal incidence of CPL, one would expect for the greatest magnitudes to result from right CPL with D-arabinose, and left CPL with L-arabinose. However, rotating the angle of incidence away from normal adds an additional form of symmetry breaking to the system, creating a bias towards one handedness of CPL, which is dependent on the direction of the incident angle. The direction of incident angle rotation for these experiments was by chance chosen to be that of a left handed CPL bias, creating a greater magnitude of optical rectification current in the presence of left CPL. As a result, the greatest magnitude of current from the four experimental conditions is expected to be produced by left CPL with L-arabinose. In contrast, the weakest optical rectification current should be observed when testing the condition of right CPL with L-arabinose, due to the use of right CPL, and opposing handedness, which both yield a lesser signal. Correspondingly, the two conditions of left CPL with D-arabinose and right CPL with L-arabinose should produce magnitudes of current that lie somewhere in the middle of this spectrum. Figure 10 summarizes the spectrum of expected magnitudes of optical rectification current.

Figure 10.

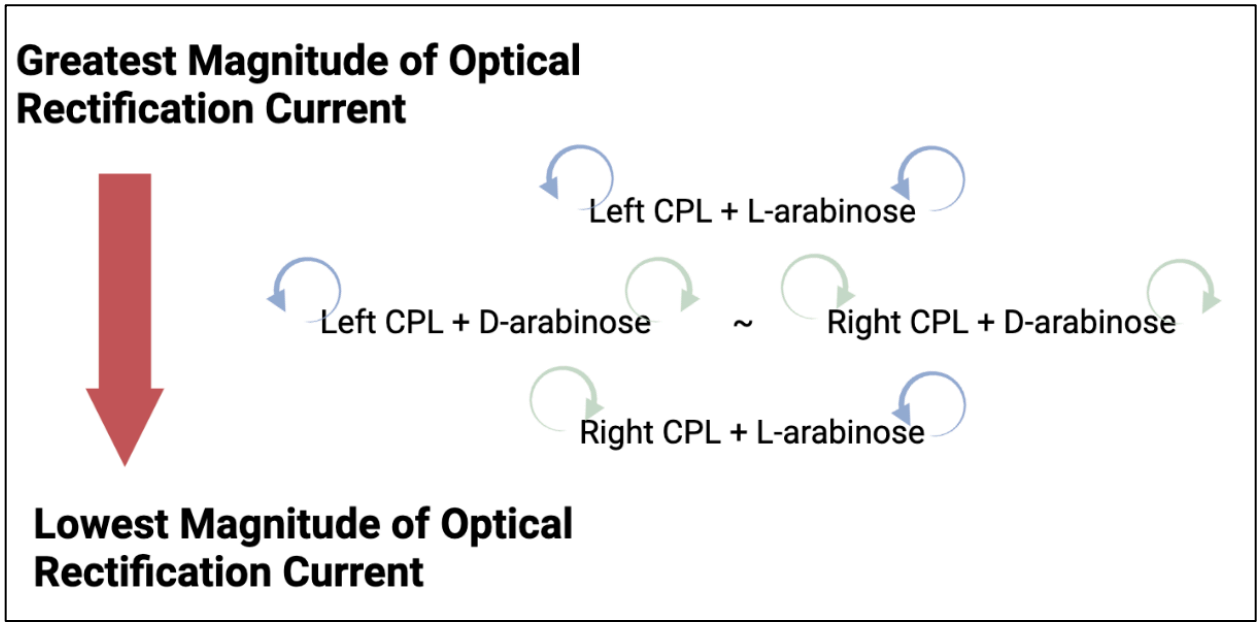

Figure 10. Summary of the approximate expectation for the relative magnitude of optical rectification current produced for each condition. Left CPL + L-arabinose and Right CPL + L-arabinose lie at the top and bottom of the spectrum, respectively. Meanwhile, Left CPL + D-arabinose and Right CPL + D-arabinose should lie somewhere in the middle, although the relative magnitude between the two is unknown.

It is through the characterization of this expectation that a measure of molecular chirality differentiation can arise. This measure is **the difference in the difference of the magnitudes of optical rectification current produced by left and right CPL resulting from the presence of L- or D-arabinose.** Figure 10 demonstrates that the difference in DC current magnitudes between left and right CPL in the presence of L-arabinose is rather large in comparison to that same difference in the presence of D-arabinose. It is the variance of these two differences that allows for enantiomeric characterization. The larger this variance is, the greater the distinction between two enantiomers. Due to the research of this enantiomeric molecular detection method being the first of its kind, the results presented should only serve as a proof of concept for the feasibility of electrically-based molecular chirality detection via optical rectification in spin momentum locking. As such, these results are not evaluated on magnitude of effect, but instead consistency findings

as a measure of success or failure. If the measured difference between left and right CPL is consistently greater in the presence of L-arabinose than in the presence of D-arabinose, the findings will support the validity of this electrical enantiomeric detection scheme.

Chapter 6: Results and Discussion

6.1 Beam Width

The 1064nm laser beam width was plotted using Mathematica and fitted to a gaussian model. (Figure 11). In the experiment, the beam path to a photodetector was initially fully blocked, causing the detectable transmitted power to be 0mW. As the blockage was removed at small intervals, increasing fractions of the beam could then pass by the edge of the blockage until the entire width of the beam was uncovered. As a result, the locations at the two ends of the steep section of the curve displayed in Figure 11 represent the locations of the edges of the horizontal diameter of the laser beam spot. From this fit, the beam width was found to be 274 μm wide, a number which comes from the width of the gaussian distribution at half of is peak magnitude. This means that the true bounds of the laser spot dissipate at a width greater than the reported measure, however, the “full width at half magnitude” generalization is the convention for defining beam width.

Figure 11.

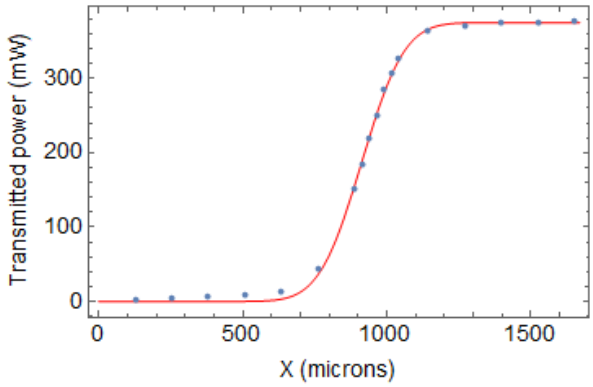

Figure 11. Graphical representation of the width of the laser beam spot at the location where it meets the gold surface.

Since the entire width of the gold grating totals only 200µm, this beam covered the entire width of the grating, and likely close to half its length. As a result, this effect may have reduced the potential for errors associated with laser spot miss alignment, however, it is also possible that this effect could have caused a reduction in the concentration of light which interacted with the gold surface as the angle of incidence grew further away from normal.

6.2 Testing Experimental Setup

Upon attempting to replicate the previous experimental findings of the lab which inspired this study, a very reassuring result was obtained (Figure 12). Here, graphical representations of the previous findings and the findings of this study demonstrate comparable results, confirming the reproducibility of the experiment, even with the addition of the cuvette setup in this study. When analyzing these figures, it is important to note the difference in horizontal axes, as the reproduced data was obtained with a range of incident angles only spanning from 0˚ to 60˚, while the original data ranges from -70˚ to 70˚. However, the reproduced findings mimic the right half of the original

surprisingly well. The two sets of data were obtained using two different laser wavelengths, attributing to some of the variances between the two datasets. However, the most notable difference between original and replica is the horizontal axis shift of the resonance peak, which was previously situated at an angle of incidence of 60˚, and is now situated at 45˚. A difference is expected of the addition of the cuvette in the experimental setup. In the event that the cuvette wall is, in deed, the culprit of this observed shift, there would be no observable effect at normal incidence, and the points would gradually shift more and more, as the angle of incidence increases, which seems consistent with the observed effect. Fortunately, whether or not the cuvette is causing a data shift, does not significantly affect any findings, since all of the data is measured with the same cuvette, causing there to be no bias when making data comparisons.

Figure 12.

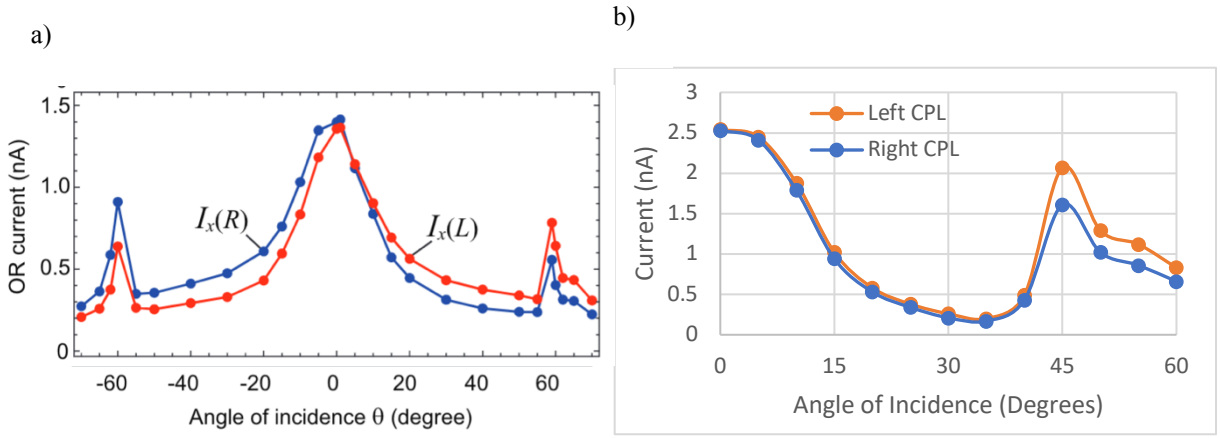

Figure 12. a) Data from the previous research from the Xu lab of optical rectification current measured as a result of left (red) and right (blue) incident CPL on the gold surface at a range of incident angles from -70˚ to 70˚. b) Data from the replicated experiment depicting the same measurements as plot a, however, with an incident angle range from 0˚ to 60˚.

The next investigation evaluated the experimental setup in a similar manner, however this time, with the inclusion of water which filled the cuvette and surrounded the gold surface grating.

The signal produced in water is expected to be much more alike with the arabinose solutions, since the arabinose solutions are mainly comprised of water and the two share almost identical refractive indexes (1.3). This signal does not have a large resonance peak where the difference between left and right CPL is amplified. Instead, it is a much smoother slope with the greatest variance between left and right CPL lying somewhere in the middle (around 30˚) (Figure 13). These findings both help to verify the functionality of the experimental setup and cuvette configuration, and provide insight into the type of data that may be expected for further experiments.

Figure 13.

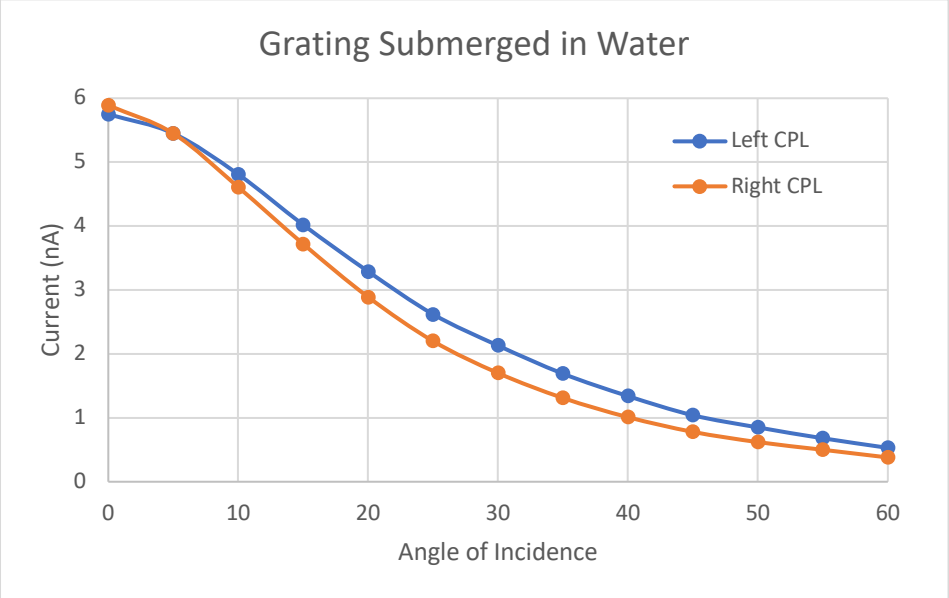

Figure 13. Values obtained for the optical rectification current resulting from left (blue) and right (red) incident CPL on the gold grating submerged in water.

6.3 Enantiomeric Molecular Detection

Two separate sets of data were collected for the optical rectification current dependency on left and right CPL in the presence of both L-arabinose and D-arabinose across a spectrum of incident angles (Figure 14). Each of these sets of data exhibits a greater magnitude of DC current resulting from incident left CPL than from incident right CPL. This outcome was anticipated due to the direction of the angle of incidence, and meets the first component of the expectation outlined in Chapter 5.

Figure 14.

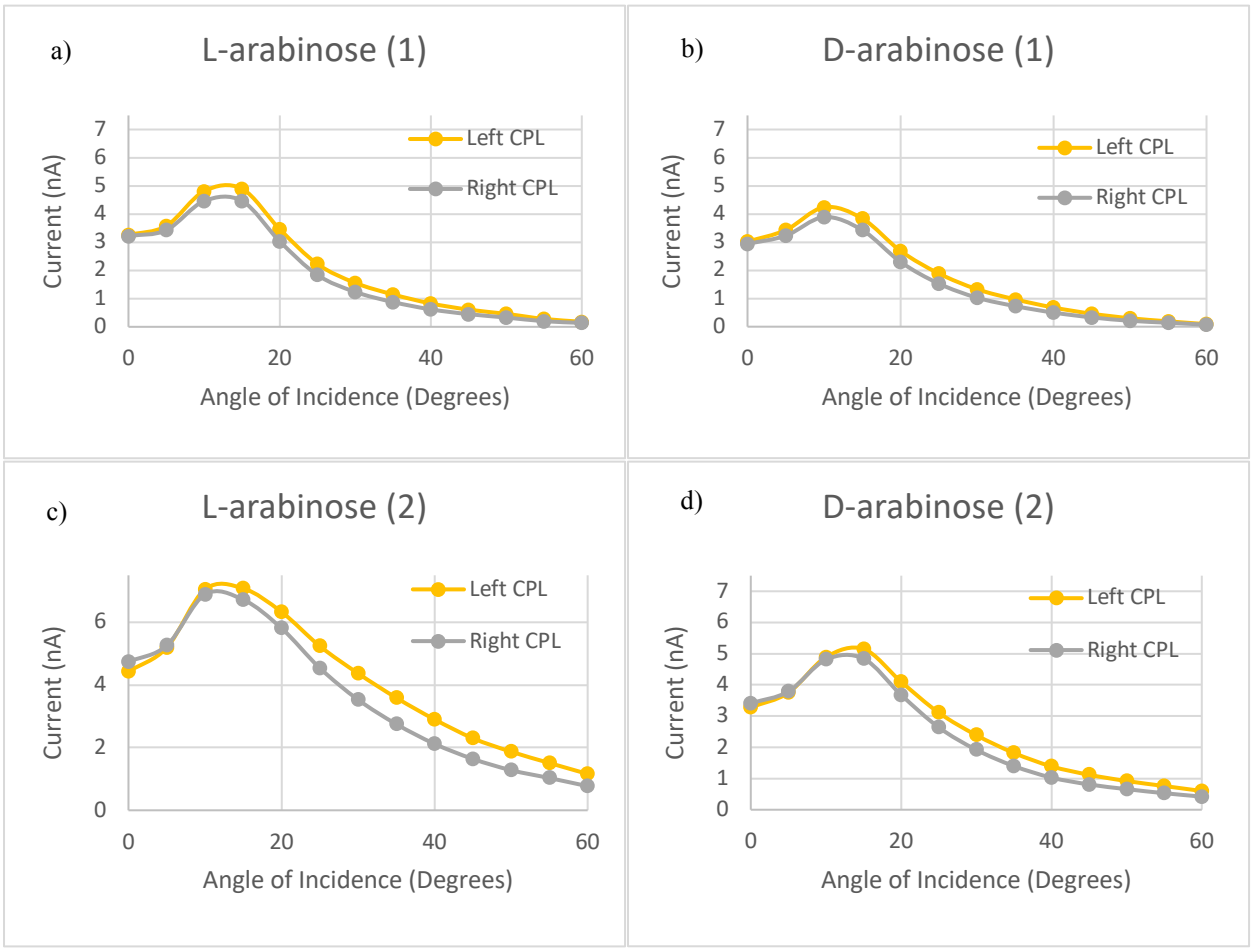

Figure 14. a) and b) depict the first sets of data for the observed optical rectification current resulting from left and right incident CPL on the gold sample in the presence of L- and D-arabinose, respectively. c) and d) plot a second set of the same measurements described for a and b.

Due to the fact that the experimental methods necessitated that the cuvette be rinsed of one solution before changing to the next, the laser needed to be realigned on the gold grating between each experimental condition. Although care was taken to position the laser as close as possible to the same location, an exact match is unlikely. Figure 15 depicts the location of the laser spot on the gold surface grating for two separate realignments. A comparison of these images shows the minute differences between the laser spot locations. As a result of these slight adjustments, it is difficult to compare the raw values of DC current magnitude from one graph to the next, however, the relative differences between optical rectification current produced by left and right CPL can still be compared amongst datasets.

Figure 15.

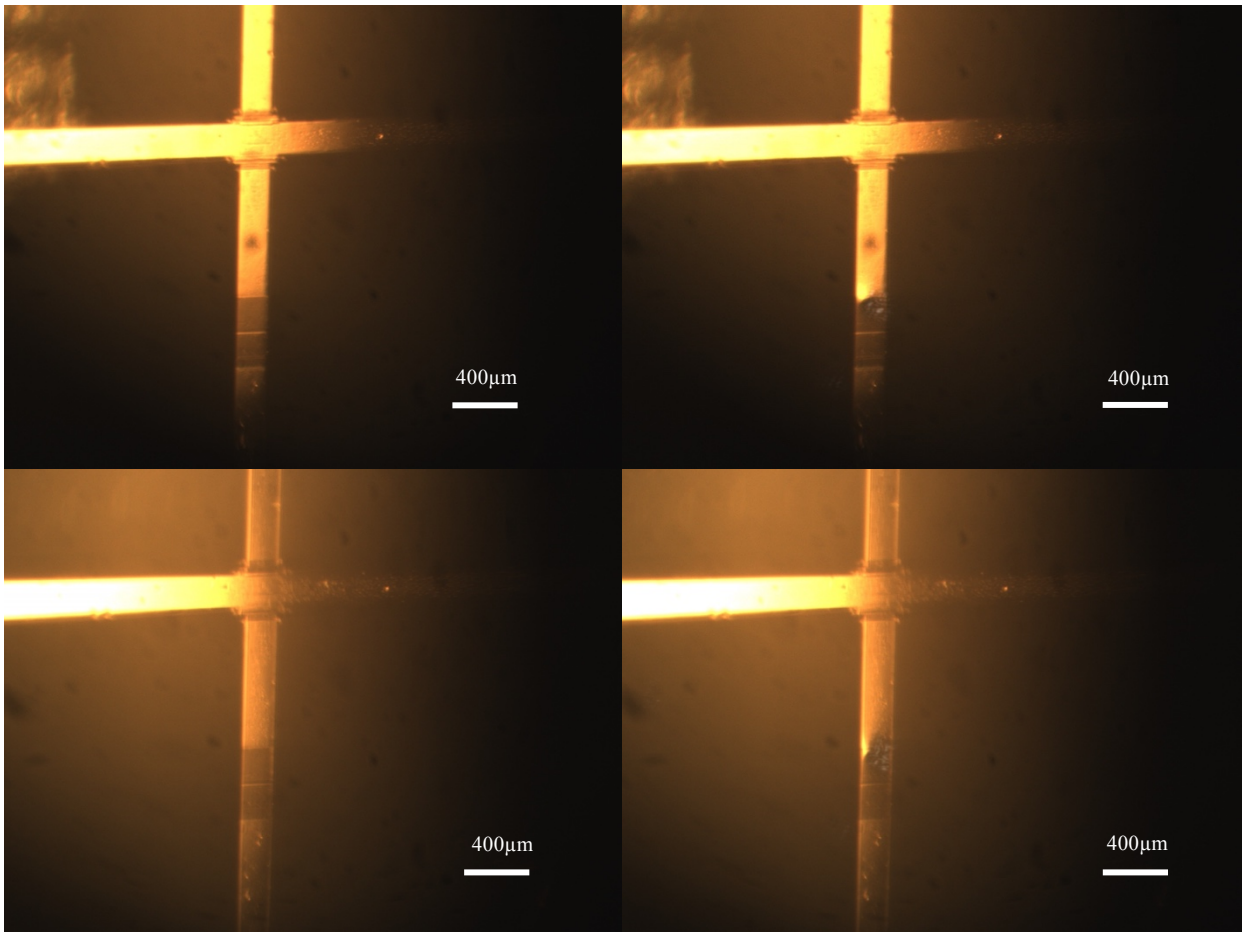

Figure 15. Microscopic images taken during data collection after two separate laser point alignments, a) and b). The gold cross in each image is the gold surface, while the grating can be seen by the small rectangle present towards the bottom of each image. Images on the left are taken with no laser beam present, while images on the right have a small laser spot, visible by the refracted light observed at the top edge of the gratings. The laser spots are aligned at approximately the same location, though there is likely a slight difference between the two locations.

Finally, the 2 plots in Figure 16 were created by subtracting the optical rectification current values corresponding to left CPL from those corresponding to right CPL for all four plots in Figure 14. These subtracted values were then plotted for L- and D-arabinose of data sets 1 and 2. As described in the Chapter 5, the question of importance here is the feasibility of electrical chiral detection of otherwise identical molecules – enantiomers, or more specifically, whether or not

these values depict a consistent peak difference between the difference of DC current produced from left and right CPL in the presence of either enantiomer, and whether that difference is indeed greater in the case of L-arabinose. Although there is a large variance in the differences of the difference of DC current, presented in Figure 16, there is a consistent trend for the two datasets in which the L-arabinose-associated values are larger on average than the values associated with D-arabinose. As a result, these findings fulfill the previously outlined conditions for experimental success, supporting the notion of feasibility for an electrically based method of chirality detection.

Figure 16.

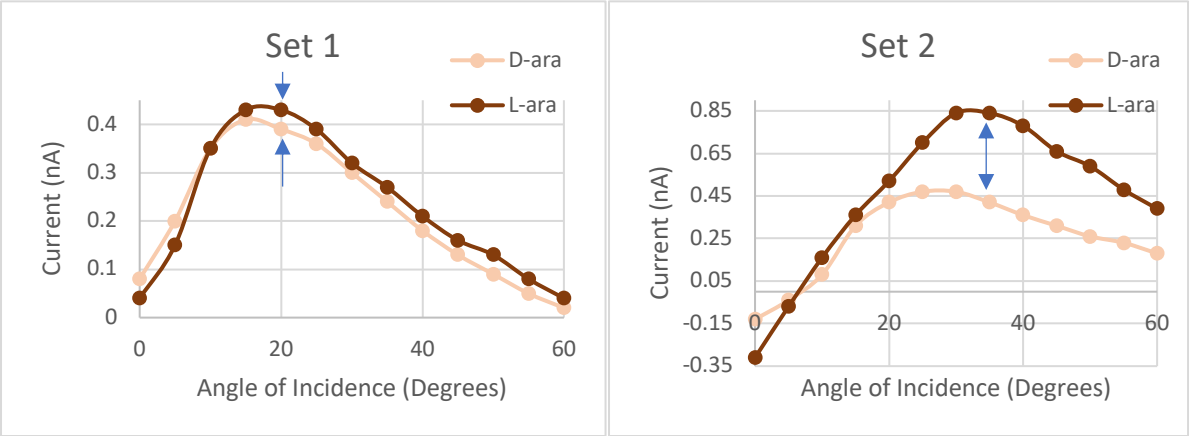

Figure 16. a) and b) depict sets one and two for the difference of optical ratification current produced from left and right CPL in the presence of L- and D-arabinose. The difference of this difference is marked by the blue arrows on each graph.

Chapter 7: Next Steps and Future Implications

As a proof-of-concept experiment, the first of the kind, it was a successful. As with any study, the repetition of results is vital for creating confidence in the significance of findings. As such, additional repetitions of this experiment are important. For similar reasons, a separate form of experimental "sanity-check," may also be called for. An experiment in which the difference in the difference between the optical rectification current produced by left and right CPL in the presence of L- and D-arabinose, but at the various concentrations of a serial dilution of each enantiomer would be a good test of the validity of the results from this study. As the two concentrations approach a molarity of zero and become essentially water, the difference between the L- and D-arabinose produced by either left or right CPL should disappear. This result would demonstrate that the results of the previous experiments were, in fact, occurring as a response to the molecular enantiomers, and not arising from some unknown reason or experimental error. Thus, this experiment would add to the significance of the current findings.

Beyond this, the next step may be to perform a dry version of this experiment. Since the molecular enantiomer source used for this study was suspended in a solution of water, the molecules are assumed to have been randomly oriented throughout the mixture. Additionally, the strength of the interaction between the SPP wave and the chiral molecules is dependent on the molecules being oriented accordingly to the SPP wave. As a result, the observed signal was likely only produced from a fraction of the molecules which happened to be oriented in the proper direction. Therefore, the immobilization of chiral molecules on the gold surface in the correct

alignment would likely intensify the observed optical rectification signal, and hopefully increase the desired detectability measurement. This experimental modification would also negate the need for the cuvette setup. This experimental setup simplification would reduce the potential for error and variability between results.

A set of parallel experiments could be envisaged on symmetric gratings and compared with the ones reported here. It is conceivable that the spin-momentum locking induced unidirectional SPP wave could suffice to differentiate the opposite chiralities via the resultant optical rectification currents.

The eventual goal of this study is to establish the electrically-based chirality detection as a viable method that is superior in size, speed, and cost to the existing ones. To the best of our knowledge, there are currently no electrically-based methods for chirality detection. A method of this sort creates the potential for the development of micro-chip sized detection devices. The research described in this thesis particularly supports the feasibility of micro-chip detection due to the superior molecular sensitivity that is produced as a result of the intensified interactions with the SPP wave in the previously-described near-field zone. Additionally, the size and cost variance associated with this electrically-based chirality detection method are a colossal improvement on those associated with the current standard methods for chirality detection, greatly enhancing the accessibility of such measurements. Finally, electrically-based detection methods present the opportunity for integration with electrical readout circuitry and silicon chips, streamlining detection processes and reducing the potential for user error. In summary, the clear benefits of electrically-based molecular enantiomer detection illustrate the necessity for further development of the described methods. We are hopeful these findings will inspire the future study and implication of the presented technology.

Bibliography

[1] Harper, D. (2022). *chiral | Etymology, origin and meaning of chiral by etymonline*. Etymonline.com. Retrieved 8 April 2022, from https://www.etymonline.com/word/chiral.

[2] Sierra, M., Sánchez, D., Gutierrez, R., Cuniberti, G., Domínguez-Adame, F., & Díaz, E. (2019). Spin-Polarized Electron Transmission in DNA-Like Systems. *Biomolecules*, *10*(1), 49. https://doi.org/10.3390/biom10010049

[3] Appelbaum, I. (2011). Introduction to spin-polarized ballistic hot electron injection and detection in silicon. *Philosophical Transactions Of The Royal Society A: Mathematical, Physical And Engineering Sciences*, *369*(1951), 3554-3574. https://doi.org/10.1098/rsta.2011.0137

[4] Bailey, J., Chrysostomou, A., Hough, J., Gledhill, T., McCall, A., & Clark, S. et al. (1998). Circular Polarization in Star- Formation Regions: Implications for Biomolecular Homochirality. *Science*, *281*(5377), 672-674. https://doi.org/10.1126/science.281.5377.672

[5] Kemp, J., Swedlund, J., Murphy, R., & Wolstencroft, R. (1971). Physical Sciences: Circularly Polarized Visible Light from Jupiter. *Nature*, *231*(5299), 169-170. https://doi.org/10.1038/231169a0

[6] Wiersema, K., Covino, S., Toma, K., van der Horst, A., Varela, K., & Min, M. et al. (2014). Circular polarization in the optical afterglow of GRB 121024A. *Nature*, *509*(7499), 201-204. https://doi.org/10.1038/nature13237

[7] Kang, J., Kang, S., Suh, J., Park, S., Yoon, D., & Lim, M. et al. (2022). Circularly Polarized Light Can Override and Amplify Asymmetry in Supramolecular Helices. *Journal Of The American Chemical Society*, *144*(6), 2657-2666. https://doi.org/10.1021/jacs.1c11306

[8] Metzger, T., Mishra, S., Bloom, B., Goren, N., Neubauer, A., & Shmul, G. et al. (2019). The Electron Spin as a Chiral Reagent. *Angewandte Chemie International Edition*, *59*(4), 1653-1658. https://doi.org/10.1002/anie.201911400

[9] Suzuki, Y. (2021). Wave packet simulations for molecular orientation induced by circularly polarized light: Toward chiral resolution in the gas phase. *Chemical Physics Letters*, *785*, 139134. https://doi.org/10.1016/j.cplett.2021.139134

[10] Finefield, J., Sherman, D., Kreitman, M., & Williams, R. (2012). Enantiomeric Natural Products: Occurrence and Biogenesis. *Angewandte Chemie International Edition*, *51*(20), 4802-4836. https://doi.org/10.1002/anie.201107204

[11] Blackmond, D. (2010). The Origin of Biological Homochirality. *Cold Spring Harbor Perspectives In Biology*, *2*(5), a002147-a002147. https://doi.org/10.1101/cshperspect.a002147

[12] Joyce, G., Visser, G., van Boeckel, C., van Boom, J., Orgel, L., & van Westrenen, J. (1984). Chiral selection in poly(C)-directed synthesis of oligo(G). *Nature*, *310*(5978), 602-604. https://doi.org/10.1038/310602a0

[13] Bastings, J., van Eijk, H., Olde Damink, S., & Rensen, S. (2019). d-amino Acids in Health and Disease: A Focus on Cancer. *Nutrients*, *11*(9), 2205. https://doi.org/10.3390/nu11092205

[14] Shinitzky, M., Shvalb, A., Elitzur, A., & Mastai, Y. (2007). Entrapped Energy in Chiral Solutions: Quantification and Information Capacity. *The Journal of Physical Chemistry B*, *111*(37), 11004-11008. https://doi.org/10.1021/jp072395f

[15] Easson, L., & Stedman, E. (1933). Studies on the relationship between chemical constitution and physiological action. *Biochemical Journal*, *27*(4), 1257-1266. https://doi.org/10.1042/bj0271257

[16] Ogston, A. (1948). Interpretation of Experiments on Metabolic processes, using Isotopic Tracer Elements. *Nature*, *162*(4129), 963-963. https://doi.org/10.1038/162963b0

[17] Davankov, V. (1997). The nature of chiral recognition: Is it a three-point interaction?. *Chirality*, *9*(2), 99-102. https://doi.org/10.1002/(sici)1520-636x(1997)9:2<99::aid-chir3>3.0.co;2-b

[18] Wan, L., Chin, A., Worley, K., & Ray, P. (2016). Cell chirality: emergence of asymmetry from cell culture. *Philosophical Transactions Of The Royal Society B: Biological Sciences*, *371*(1710), 20150413. https://doi.org/10.1098/rstb.2015.0413

[19] Davies, N., & Teng, X. (2003). Importance of Chirality in Drug Therapy and Pharmacy Practice: Implications for Psychiatry. *Advances In Pharmacy*, *I*(3), 242-252. Retrieved 11 April 2022, from.

[20] US Food and Drug Administration. (1973). *Code of Federal Regulations 21:1308*. Washington, DC: US Government Printing Office.

[21] Wsol, V., Skalova, L., & Szotakova, B. (2004). Chiral Inversion of Drugs: Coincidence or Principle?. *Current Drug Metabolism*, *5*(6), 517-533. https://doi.org/10.2174/1389200043335360

[22] Piossek, C., Thierauch, K., Schneider-Mergener, J., Volkmer-Engert, R., Bachmann, M., & Korff, T. et al. (2003). Potent inhibition of angiogenesis by D,L-peptides derived from

vascular endothelial growth factor receptor 2. *Thrombosis And Haemostasis*, *90*(09), 501-510. https://doi.org/10.1160/th03-02-0106

[23] Werle, M., & Bernkop-Schnürch, A. (2006). Strategies to improve plasma half life time of peptide and protein drugs. *Amino Acids*, *30*(4), 351-367. https://doi.org/10.1007/s00726-005-0289-3

[24] Kalíková, K., Šlechtová, T., & Tesařová, E. (2016). Enantiomeric Ratio of Amino Acids as a Tool for Determination of Aging and Disease Diagnostics by Chromatographic Measurement. *Separations*, *3*(4), 30. https://doi.org/10.3390/separations3040030

[25] Sasabe, J., Chiba, T., Yamada, M., Okamoto, K., Nishimoto, I., Matsuoka, M., & Aiso, S. (2007). D-Serine is a key determinant of glutamate toxicity in amyotrophic lateral sclerosis. *The EMBO Journal*, *26*(18), 4149-4159. https://doi.org/10.1038/sj.emboj.7601840

[26] MacKay, M., Kravtsenyuk, M., Thomas, R., Mitchell, N., Dursun, S., & Baker, G. (2019). D-Serine: Potential Therapeutic Agent and/or Biomarker in Schizophrenia and Depression?. *Frontiers In Psychiatry*, *10*. https://doi.org/10.3389/fpsyt.2019.00025

[27] Hu, B., Huang, K., Zhang, X., Zhang, P., & Yu, S. (2015). Solubility and Seeded Metastable Zone width of functional sugar L-arabinose. *Food Science And Technology (Campinas)*, *35*(1), 51-57. https://doi.org/10.1590/1678-457x.6329

[28] Hu, B., Huang, K., Zhang, X., Zhang, P., & Yu, S. (2015). Solubility and Seeded Metastable Zone width of functional sugar L-arabinose. *Food Science And Technology (Campinas)*, *35*(1), 51-57. https://doi.org/10.1590/1678-457x.6329

[29] Yu, L., Wang, S., & Zeng, S. (2012). Chiral Mobile Phase Additives in HPLC Enantioseparations. *Methods In Molecular Biology*, 221-231. https://doi.org/10.1007/978-1-62703-263-6_13

[30] Teixeira, J., Tiritan, M., Pinto, M., & Fernandes, C. (2019). Chiral Stationary Phases for Liquid Chromatography: Recent Developments. *Molecules*, *24*(5), 865. https://doi.org/10.3390/molecules24050865

[31] Patil, R., Weatherly, C., & Armstrong, D. (2018). *Chiral Analysis: Advances in Spectroscopy, Chromatography, and Emerging Methods* (2nd ed., pp. 469-506). Elsevier.

[32] Perez, E., Knapp, J., Horn, C., Stillman, S., Evans, J., & Arfsten, D. (2016). Comparison of LC–MS-MS and GC–MS Analysis of Benzodiazepine Compounds Included in the Drug Demand Reduction Urinalysis Program. *Journal Of Analytical Toxicology*, *40*(3), 201-207. https://doi.org/10.1093/jat/bkv140

[33] El-Khoury, J. (2018). *Financial considerations for purchasing a mass spectrometer*. Presentation, Palm Springs, CA. https://www.msacl.org/presenter_slides/2018_US_deborah.french_82527_slides.pdf.

[34] Harvie, A., Phillips, T., & deMello, J. (2020). A high-resolution polarimeter formed from inexpensive optical parts. *Scientific Reports*, *10*(1). https://doi.org/10.1038/s41598-020-61715-7

[35] Watson, J. (2004). *Molecular biology of the gene* (5th ed., p. 503). Pearson.

[36] Hu, B., Huang, K., Zhang, X., Zhang, P., & Yu, S. (2015). Solubility and Seeded Metastable Zone width of functional sugar L-arabinose. *Food Science And Technology (Campinas)*, *35*(1), 51-57. https://doi.org/10.1590/1678-457x.6329

Appendix

Section I.

Purchase Sites and Grades of L- and D-arabinose.

L-arabinose:

Vendor: GoldBio

Item Number: A-300-100

Grade: Molecular Biology Grade

D-arabinose:

Vendor: MilliporeSigma

Item Number: A3131-100G

Grade: ≥ 98% purity

Section II.

Wolfram Mathematica code for gaussian fit of laser beam width measurements.

Beam Width of 1064.nb - Wolfram Mathematica 12.1

File Edit Insert Format Cell Graphics Evaluation Palettes Window Help

```
In[8]:= LaserFoc15 = {{127, 3}, {254, 4}, {381, 6}, {508, 8}, {635, 14}, {762, 43}, {889, 152}, {914.4, 185}, {939.8, 219}, {965.2, 251}, {990.6, 284}, {1016, 307}, {1041.4, 327}, {1143, 363}, {1270, 371}, {1397, 374}, {1524, 376}, {1651, 377}};

In[9]:= Length[LaserFoc15]
Out[9]= 18

In[12]:= plotdata1 = ListPlot[LaserFoc15]
```

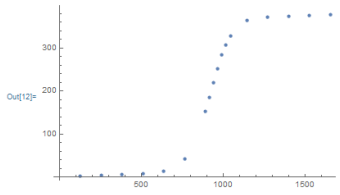

Out[12]=

```
In[14]:= Ffit[X_, x0_, w_] := ∫_0^X Exp[-(x - x0)^2 / w^2] dx

In[15]:= Fit1 = NonlinearModelFit[LaserFoc15, AA Ffit[X, x0, w], {{AA, 0.1}, x0, w}, X]
Out[15]= FittedModel[187.46 (1. + Erf[0.00606756 (-913.475 + X)])]

In[18]:= plotfit1 = Plot[Fit1[X], {X, 0, 1670}, PlotStyle → Red];

In[20]:= PlotA = Show[plotfit1, plotdata1, Frame → True, Axes → False, FrameLabel → {"X (microns)", "Transmitted power (mW)"}, LabelStyle → {Black, Larger}]
```

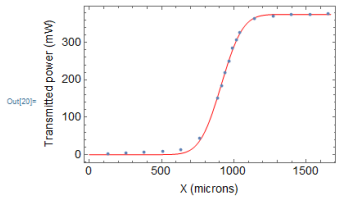

Out[20]=

```
In[21]:= Fit1["ParameterTable"]
```

	Estimate	Standard Error	t-Statistic	P-Value
AA	1.28345	0.038424	33.4023	1.69732×10^{-15}
x0	913.475	2.16484	421.961	5.59771×10^{-32}
w	164.811	5.2274	31.5283	3.9896×10^{-15}

Out[21]=

```
In[22]:= FWHM1mm = (w /. Fit1["BestFitParameters"]) 2 √Log[2]
Out[22]= 274.428
```

Section III

Raw Data

i) Replication of previous experimental findings, with addition of cuvette

angle of incidence	*Left CPL*	*Right CPL*
0	2.54	2.53
5	2.45	2.41
10	1.88	1.79
15	1.02	0.94
20	0.58	0.53
25	0.38	0.34
30	0.26	0.21
35	0.2	0.17
40	0.49	0.43
45	2.07	1.61
50	1.29	1.02
55	1.12	0.86
60	0.83	0.66

a) Differences between left and right CPL of above

angle of incidence	*Left - Right CPL*
0	0.01
5	0.04
10	0.09
15	0.08
20	0.05
25	0.04
30	0.05
35	0.03
40	0.06
45	0.46
50	0.27
55	0.26

60	0.17

ii) Grating submerged in pure deionized water

angle of incidence	*Left CPL*	*Right CPL*
0	5.75	5.89
5	5.45	5.45
10	4.81	4.61
15	4.02	3.72
20	3.29	2.89
25	2.62	2.2
30	2.13	1.7
35	1.69	1.31
40	1.34	1.01
45	1.04	0.78
50	0.85	0.62
55	0.68	0.5
60	0.53	0.38

b) Differences between left and right CPL of above

angle of incidence	*Left - Right CPL*
0	0.14
5	0
10	-0.2
15	-0.3
20	-0.4
25	-0.42
30	-0.43
35	-0.38
40	-0.33
45	-0.26
50	-0.23
55	-0.18
60	-0.15

iii) DC current in the presence of L-arabinose (set 1)

angle of incidence	*Left CPL*	*Right CPL*
0	3.26	3.22
5	3.58	3.43
10	4.81	4.46
15	4.9	4.47
20	3.47	3.04
25	2.23	1.84
30	1.56	1.24
35	1.15	0.88
40	0.83	0.62
45	0.61	0.45
50	0.46	0.33
55	0.28	0.2
60	0.18	0.14

c) Differences between left and right CPL of above

angle of incidence	*Left - Right CPL*
0	0.04
5	0.15
10	0.35
15	0.43
20	0.43
25	0.39
30	0.32
35	0.27
40	0.21
45	0.16
50	0.13
55	0.08
60	0.04

iv) DC current in the presence of L-arabinose (set 2)

angle of incidence	*Left CPL*	*Right CPL*
0	4.43	4.74
5	5.19	5.26
10	7.05	6.89
15	7.08	6.72

20	6.33	5.81
25	5.24	4.54
30	4.37	3.53
35	3.59	2.75
40	2.9	2.12
45	2.3	1.64
50	1.87	1.28
55	1.51	1.03
60	1.16	0.77

d) Differences between left and right CPL of above

angle of incidence	*Left – Right CPL*
0	-0.31
5	-0.07
10	0.16
15	0.36
20	0.52
25	0.7
30	0.84
35	0.84
40	0.78
45	0.66
50	0.59
55	0.48
60	0.39

v) DC current in the presence of D-arabinose (set 1)

angle of incidence	*Left CPL*	*Right CPL*
0	3.02	2.94
5	3.43	3.23
10	4.24	3.89
15	3.84	3.43
20	2.69	2.3
25	1.89	1.53
30	1.33	1.03
35	0.97	0.73
40	0.68	0.5

45	0.46	0.33
50	0.3	0.21
55	0.19	0.14
60	0.09	0.07

e) Differences between left and right CPL of above

angle of incidence	*Left – Right CPL*
0	0.08
5	0.2
10	0.35
15	0.41
20	0.39
25	0.36
30	0.3
35	0.24
40	0.18
45	0.13
50	0.09
55	0.05
60	0.02

vi) DC current in the presence of D-arabinose (set 2)

angle of incidence	*Left CPL*	*Right CPL*
0	3.28	3.41
5	3.75	3.79
10	4.89	4.81
15	5.15	4.84
20	4.1	3.68
25	3.11	2.64
30	2.39	1.92
35	1.82	1.4
40	1.39	1.03
45	1.12	0.81
50	0.92	0.66
55	0.76	0.53
60	0.6	0.42

f) Differences between left and right CPL of above

angle of incidence	*Left – Right CPL*
0	-0.13
5	-0.04
10	0.08
15	0.31
20	0.42
25	0.47
30	0.47
35	0.42
40	0.36
45	0.31
50	0.26
55	0.23
60	0.18